Journal of Magnetism and Magnetic Materials 477 (2019) 372–381

Contents lists available at ScienceDirect

Journal of Magnetism and Magnetic Materials

journal homepage: www.elsevier.com/locate/jmmm

Review Articles

Effect of manganese in high silicon alloyed non-oriented electrical steel sheets

M. Schulte[a,*], S. Steentjes[b], N. Leuning[b], W. Bleck[a], K. Hameyer[b]

[a] Steel Institute, RWTH Aachen University, D-52072 Aachen, Germany
[b] Institute of Electrical Machines (IEM), RWTH Aachen University, D-52062 Aachen, Germany

ARTICLE INFO

Keywords:
Electrical steel
Manganese
Core loss
Grain growth
Texture

ABSTRACT

The effect of manganese on high silicon alloyed electrical steel sheets has been investigated. Three alloys with different Mn content (0.20, 0.69 and 1.38 wt%) have been melted on a laboratory scale and processed to fully-finished electrical steel sheets with 0.5 mm thickness. The effect of Mn on the mechanical, microstructural and magnetic properties has been studied. The average grain size decreases as Mn content increases. The texture is hardly affected by a variation of Mn content but the material is strengthened with increasing Mn content by solid solution strengthening. Mn increases the electrical resistance, which results in lower core losses at higher frequencies.

1. Introduction

Non-oriented (NO) electrical steel sheets are in terms of annually produced tons the most important soft magnetic material [1–3]. They are mainly used in rotating electrical machines like motors and generators to carry the magnetic flux. For energy saving purposes, there is an increasing demand for materials with low magnetic losses, i.e. to produce higher-efficiency motors. Simultaneously, a high magnetic induction and a high magnetic permeability are essential, in particularly when taking into account the trend to smaller motor dimensions. On the other hand high strength electrical steels are necessary for bearing higher centrifugal forces in rotors [4,5].

Many attempts have been made to satisfy increasing demands of electrical steels, e.g., by reducing thickness, manipulation of texture and microstructure, strip casting and the adaptation of material processing [6–11]. Another way is the arrangement of the chemical composition, because magnetic and mechanical properties of NO electrical steels are strongly affected by alloying elements [12–14]. Studies about the effect of alloying elements on material properties are mainly focused on silicon (Si) and aluminium (Al). But the possibility to produce grades, which have very low contents of unwanted tramp elements such as sulfur (S), nitrogen (N) and oxygen (O) allows metallurgists more freedom in alloy design, nowadays [15].

One element of choice in case of alloying is manganese (Mn), because it has the potential to increase the electrical resistivity and thereby reducing losses. If the S content is low, unwanted MnS precipitations can be avoided and Mn stays in solid solution [16] showed that Mn additions in a range of 0.25–0.64 wt% in a Si free steel decreases losses linearly (2.40 W/wt% Mn) and increases permeability and grain growth. Liao [17] found improved magnetic properties for electrical steels with 0.3–1.25 wt% Mn in Si free steels while higher Mn content causes smaller grains, which deteriorates the magnetic losses. In [18] a decrease of grain size after final annealing (FGS) and increase in {2 2 2} texture component due to $MnSiN_2$ precipitations in ultra-low S grades with 0.5 wt% Si was found. The amount of MnS precipitations keeps stable with increasing Mn content up to 0.94 wt%. In [19] a texture improvement by 0.5 wt% Mn in high Si alloyed electrical steels was reported. Same is shown in [20] by alloying 1.3 wt% Mn in high purity 0.5 wt% Si steel. While Mn content increases, core loss decreases significantly and magnetic induction increases slightly at the same time. Contradictory, Kubota [4] found a decrease of magnetic induction and an increase of core losses for up to 2.0 wt% Mn in 3.0 wt% Si steel. Yield strength increases by solid solution strengthening of around 33 MPa/1 wt% Mn but no mention was made of the exact chemical composition of the material. Increasing S content deteriorates the material properties at each Mn level [21]. Very low S and O contents are essential for Mn alloyed electrical steels to keep Mn in solid solution and to avoid Mn precipitations like oxides and sulfides [22].

The results so far are very contradictory and the pure effect of Mn in high silicon alloyed electrical steel has not been well studied in steels with present-day very low levels of tramp elements. Therefore, in this work, the effect of Mn in 2.66 wt% Si electrical steels is examined with

* Corresponding author at: Steel Institute, RWTH Aachen University, Intzestr. 1, 52072 Aachen, Germany.
E-mail address: markus.schulte@iehk.rwth-aachen.de (M. Schulte).

https://doi.org/10.1016/j.jmmm.2018.07.025
Received 27 March 2018; Received in revised form 25 June 2018; Accepted 9 July 2018
Available online 10 July 2018
0304-8853/

Table 1
Chemical compositions in wt%. *measured by combustion analysis.

Spec.	C*	Si	Mn	P	S*	Al	N*	O*
Mn0.2	0.0029	2.66	**0.20**	0.014	0.0003	0.004	0.0002	0.0045
Mn0.7	0.0025	2.66	**0.69**	0.014	0.0004	0.004	0.0002	0.0082
Mn1.4	0.0047	2.66	**1.38**	0.014	0.0014	0.005	0.0002	0.0085

regard to the magnetic, mechanical and microstructural properties. The obtained results support the alloy design of new electrical steels.

2. Experimental procedure

Three ingots of 70 kg each were produced by vacuum induction melting. The Mn content varied in a range of 0.2–1.38 wt% while other elements were kept constant. Chemical compositions are shown in Table 1. Carbon content was chosen as low as possible because it worsens the magnetic properties in electrical steels, especially due to magnetic aging caused by carbide precipitation [23]. Mn levels were adjusted in a range from a common Mn value in electrical steels of 0.2 wt% over 0.69 wt% up to 1.38 wt% to meet the requirements regarding the electrical resistance of comparable Al alloyed grades. S and N contents are as low as possible. The increase of S in Mn1.4 is caused by the high content of Mn because even high purity Mn flakes contain some S. Mn flakes contain S. The Al content in the range of ≤ 50 ppm reflects modern steel shop practice.

The ingots were hot forged to 100 mm × 100 mm cross section to destroy the dendritic casting structure and to homogenize the material. Hot rolling was performed starting with 20 mm thick plates down to around 2.2 mm hot sheet thickness in six rolling passes. Slab reheating temperature was 1150 °C for 20 min. The finishing temperature of hot rolling was 700 °C and the hot-rolled specimens were covered by insulating material to simulate the cooling practice of industrial produced coils. After that, the specimens were pickled in hydrochloride acid to remove oxide layers. Scale free samples were successfully cold rolled on a laboratory mill to 0.5 mm thickness. Samples were hot sheet annealed (HSA) in a batch furnace at 740 °C for 20 h on hydrogen atmosphere before cold rolling. Final annealing for all samples was performed in a salt bath at 1000 °C to obtain recrystallization and grain growth with subsequent air cooling. The according *T-t*-diagram is given in Fig. 1.

Magnetic properties were measured by Brockhaus MPG200D single sheet tester (SST) on 60 mm × 60 mm samples in rolling (RD) and transverse direction (TD). To obtain reliable values, three samples of each condition were measured and all values (RD, TD) were averaged. The total losses P_t were separated in hysteresis losses P_h, eddy-current losses P_e and anomalous losses P_a according to the loss separation principle. The examined range of frequency was from 10 Hz up to 1000 Hz with 50 Hz, 100 Hz, 200 Hz, 400 Hz and 700 Hz as intermediate steps. As modern electrical drives especially for e-mobility work at high frequencies, the material properties for those frequencies are of growing importance and are therefore considered in this study. Specific electrical resistances were measured according to IEC 60404-13.

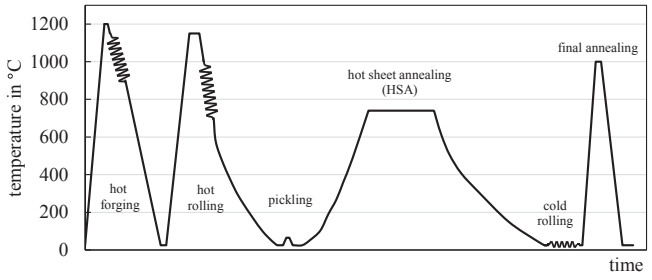

Fig. 1. Thermo-mechanical process used in this study.

Microstructural characterization was performed by light and electron microscopy. Phase transformation was examined by Bähr DIL 805 A/D using a heating rate of 1.8 K/min. Chemical characterization of precipitations was made by EDX technique. Average grain size was measured using linear intercept method along the rolling direction. Texture was identified by X-ray technology using a Bruker D8 Advance diffractometer equipped with texture goniometer. The new surface after removing 25% of the sheet thickness was taken as the layer for texture measurement. Orientation distribution functions (ODF) were calculated from {011}, {002} and {112} pole figures and the fibre volume fractions of characteristic fibre textures were measured.

Mechanical properties were determined in RD by tensile test using a Zwick Z 100 machine attached with video extensometer. Applied strain rate was 0.45 mm/min for A30 sample geometry with a measuring length of 20 mm.

3. Results and discussion

3.1. Microstructure

Mn is an austenite forming element which leads to thermodynamic stabilization of austenite. For electrical steels, a single ferrite phase material without ferrite/austenite phase transformation enables high temperature annealing. The dilatation curves of Mn0.7 and Mn1.4 are shown in Fig. 2a. The Curie-temperature T_C is 733 °C and 729 °C for Mn0.7 and Mn1.4 respectively which causes a slight deviation of the linear slope of the dilatation curves. No phase transformation is observed which is comparable to high Si alloyed grades with low Mn content even though ThermoCalc equilibrium calculations show a Ferrite to Austenite phase transformation for Mn1.4 (Fig. 2b). Due to the very low heating rate of 1.8 K/min, which is used for the determination of the dilatation curves, a fully ferritic structure without phase transformation can be expected in technical processes because continuous annealing furnaces have higher heating rates. Therefore, the chosen final annealing temperature of 1000 °C is feasible to achieve recrystallization and grain growth.

As grain size is a crucial factor especially for P_h and P_a because grain boundaries interact with domain walls and their size is determined by the grain size, it needs to be analyzed. Microstructures of the examined materials with hot sheet annealing and final annealing at 1000 °C for 120 s are shown in Fig. 3. They all have a typical uniform, coarse grain structure.

HSA leads to recrystallization of the hot sheet which itself shows a pancake type rolling microstructure with deformed and elongated grains in rolling direction and deformation bands due to a relative low final rolling temperature. The according micrographs are shown in Fig. 4. The grain structure after HSA is not homogenous through the entire thickness. Grain size increases from the surface to the center of the specimens where occasionally some unrecrystallized grains occur. This could be the result of an inhomogeneous deformation structure caused by rolling, which leads to a higher shear strength in the near surface areas of the sheet. So nucleation takes place at the same time in many different positions resulting in mutual disability for grain growth. Additionally, a lower heating rate in the center of the sheet allows recovery before recrystallization so that the number of nuclei for recrystallization is reduced there, which promotes bigger grains after recrystallization.

Grain size development by isothermal heat treatment is shown in Fig. 5. Mn0.2 has the highest grain size after each heat treatment and grain size decreases with increasing Mn content. Temperature is the determining factor on grain size compared to annealing time 800 °C are sufficient for recrystallization but grain growth is limited. Grain growth rate slows down with increasing annealing time. This is a result of decreasing grain boundary area per volume fraction, which stores most of the energy of the material. If the interfacial energy decreases, the driving force for grain growth also decreases [24].

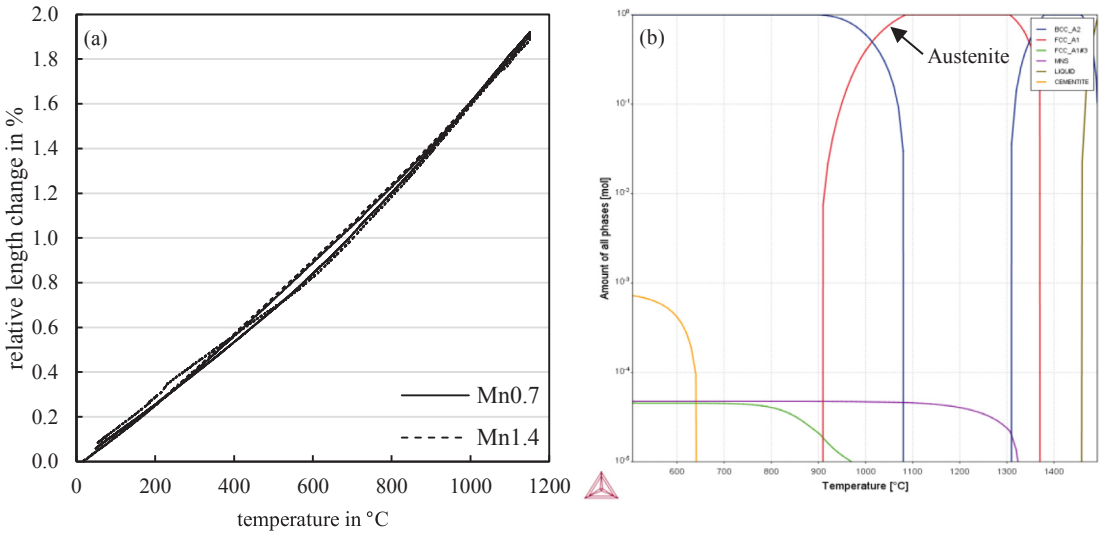

Fig. 2. a) Dilatation curves of Mn0.7 and Mn1.4b) ThermoCalc equilibrium calculations for Mn1.4.

The kinetics of grain growth during isothermal heat treatment can generally be described by empirical Eq. (1) [25,26]:

$$d_t^n - d_0^n = K \cdot t \quad (1)$$

Following the assumption that diffusion of atoms across the grain boundary is a simple activated process [27], the Arrhenius Eq. (2) is valid which means:

$$K = k_0 \cdot \exp\left(-\frac{Q}{RT}\right), \quad (2)$$

where d_t is the grain size after isothermal annealing time t, d_0 is the grain size after recrystallization, Q is the activation energy, R the universal gas constant, K and k_0 are constants and T is the absolute temperature. For these calculations the grain growth exponent of $n = 2$ is selected. This value is taken from the standard model of normal grain growth according to [25] and [26]. The measured grain size d_0 is 12.2 µm, 11.3 µm and 9.4 µm for Mn0.2, Mn0.7 and Mn1.4 respectively. For the calculations of the temperature independent parameters k_0 and Q, the grain sizes after 300 s holding time are chosen. The Arrhenius plot in Fig. 6a shows a linear behavior with high coefficients of determination $R^2 > 0.998$. The slope of the lines is $-Q/R$ and the resulting activation energies are 200 kJ, 185 kJ and 175 kJ for Mn0.2, Mn0.7 and Mn1.4 respectively. As the grain growth rate is a function of both, Q and k_0, the grain growth behavior cannot be described by Q solely. Therefore, the grain growth rate is presented in Fig. 6b depending on temperature and material. The grain growth rate has an exponential course of curve with increasing temperature. Increasing Mn content causes a decrease of grain growth rate. The effect on grain growth rate decreases with increasing Mn content. As Mn is a solute element, it tends to segregate to grain boundaries to lower its energy. When it comes to grain boundary migration, the solute drag effect occurs [26].

When K is determined, grain growth evoked by isothermal heat treatment can be estimated from the general equation for different holding times and temperature. The resulting FGS are shown in Fig. 7.

Besides grain size, precipitates and inclusions also affect the magnetic properties [23,28]. Depending on their size, they can influence the magnetic properties indirectly by harming grain size and directly by the interaction with domain walls. Fig. 8 shows some characteristic precipitations of the different materials.

In Mn0.2 just Al-Si oxides could be detected (Fig. 8a). Their size is of a few µm. Mn0.7 contains additionally to Al-Si oxides some MnS which is shown in Fig. 8b. Their sizes are < 1 µm. MnS precipitations can also be found in Mn1.4 and their number is highest of all materials there. This is a consequence of the higher S content in Mn1.4. The MnS precipitation size is also below one µm there. Precipitations having this size in the range of nm are able to interact with grain boundaries which can be seen in (Fig. 8c) following that MnS precipitation might harm grain growth during final annealing. Mn1.4 also contains Al-Si oxides as increasing Mn content benefits the oxygen absorption of the melt during the metallurgical melting process. Therefore the total oxygen content increases and the number of formed oxides increases also. Some of the oxides in Mn1.4 are enriched by Mn which can be seen in Fig. 8d. The oxides are mainly found in clusters and spread along the rolling direction, which is a hint that they were big oxides formed from the liquid melt before rolling. Due to very low content of N, no nitrides could be found in any of these steels. The increasing amount of second phase particles with increasing Mn content is presented in Fig. 9a but the distribution of the particle size is not affected by Mn content which can be seen in Fig. 9b.

The MnS precipitations in steels Mn0.7 and Mn1.4 appear just very occasionally. The reason is that HSA temperature and final annealing temperature are not high enough to dissolve precipitations in the hot sheet. According to ThermoCalc calculation, the dissolution temperature of MnS is 1050 °C, 1150 °C and 1330 °C for Mn0.2, Mn0.7 and Mn1.4 respectively. So they cannot precipitate again during heat treatment processes which would affect their number and size. But thinkable is an increasing size of MnS precipitations by heat treatment

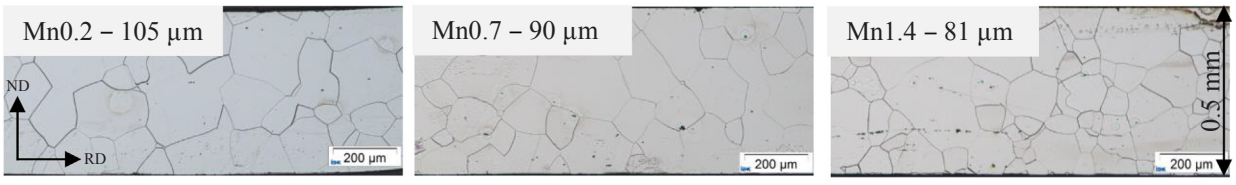

Fig. 3. Microstructure of Mn0.2, Mn0.7 and Mn1.4 after final annealing at 1000 °C with annealing time of 120 s.

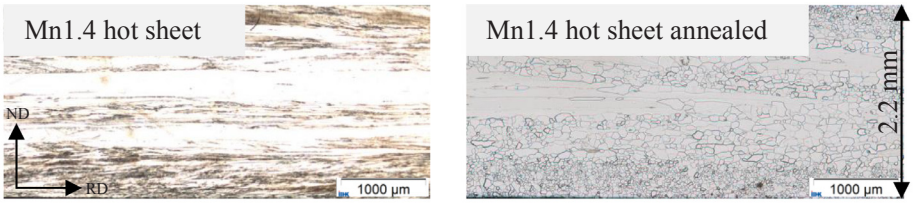

Fig. 4. Microstructure of Mn1.4 after hot rolling (left) and after hot sheet annealing (right).

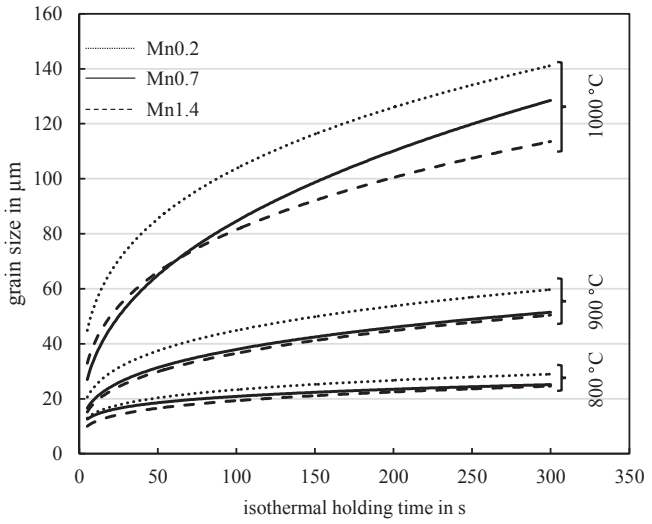

Fig. 5. Grain growth during isothermal heat treatment at 800 °C, 900 °C and 1000 °C.

which was proven in [29].

Recrystallization textures after final annealing are presented in Fig. 10 as $\varphi_2 = 45^\circ$ orientation distribution function (ODF) sections of Euler space on the $S = 0.5$ layer. This section of the Euler space represents almost all texture components which are observed in recrystallized or cold rolled bcc steels to which the investigated ones belong.

According to the $\varphi_2 = 45^\circ$ orientation distribution function (ODF) sections, the fibre volume fraction of relevant textures can be determined (Fig. 11). The gamma fibre is the dominant texture component of around 13% and its fraction is slightly decreased by Mn alloying. The gamma fibre comprises the {1 1 1} ⟨uvw⟩ orientations with {1 1 1} parallel to the normal direction (ND) of the sheet plane. Due to the anisotropic behavior of magnetization of the crystal, these orientations deteriorate the magnetizability of the steel sheets and need to be avoided. Unfortunately, the gamma fibre is the typical recrystallization texture of bcc materials. Optimum conditions for nucleation during recrystallization are within the as-deformed microstructure, which have the highest stored energy [30]. This occurs in grains with gamma fibre orientations. There, the driving force for recrystallization is higher compared to grains with other orientations. Grains with gamma fibre orientation begin to grow at the expense of other orientations which might cause its high measured fraction [31]. The alpha fibre volume fraction decreases with increasing Mn content but the theta fibre, which is the most favorable texture component because of it has two coplanar ⟨1 0 0⟩ directions in the sheet plane, is not remarkably affected. The eta fibre fraction decreases for Mn0.7 and increases with higher Mn fractions.

To quantify the texture of NO electrical steel, Kestens [32] introduced the A_θ parameter which can be derived from the ODF. It can occur in a range of 0–54.7 deg and describes the minimum angle between the applied field direction and the closest ⟨1 0 0⟩ direction of the crystal. As the magnetic field direction in NO electrical steel sheet changes its direction, a direction averaged A parameter needs to be calculated by integration over A_θ which results in a theoretically lowest A parameter of 22.5 deg. This value would occur if there are solely orientations belonging to the theta fibre in the material. This implies that a low A parameter is linked to a high texture quality. The possible range of the A parameter is 22.5 (theta fibre) − 38.7 deg (gamma fibre).

As shown in Fig. 12, Mn0.2 has the highest A_θ values for each field direction angle. Mn0.7 shows a similar trend like Mn0.2 with slightly lower A_θ values in general. For the angles close to RD and TD direction, Mn1.4 has favorable A_θ values but for angles between 25 and 52 deg, Mn0.7 has the best A_θ values. Lowest A_θ values for all materials exist in

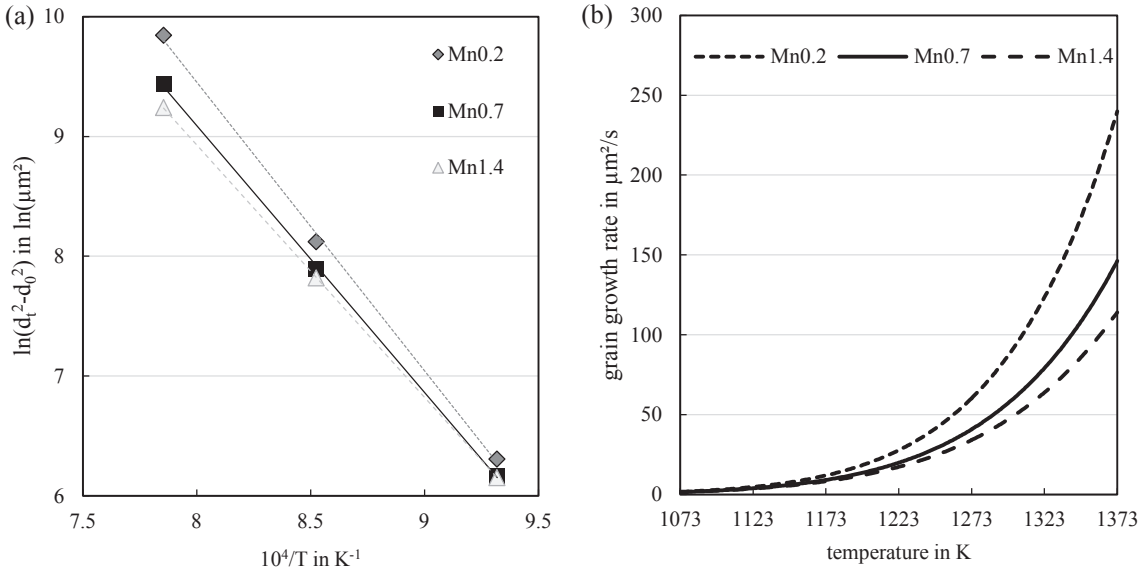

Fig. 6. Determination of Q from Arrhenius plot a) and the resulting grain growth rate depending on temperature b).

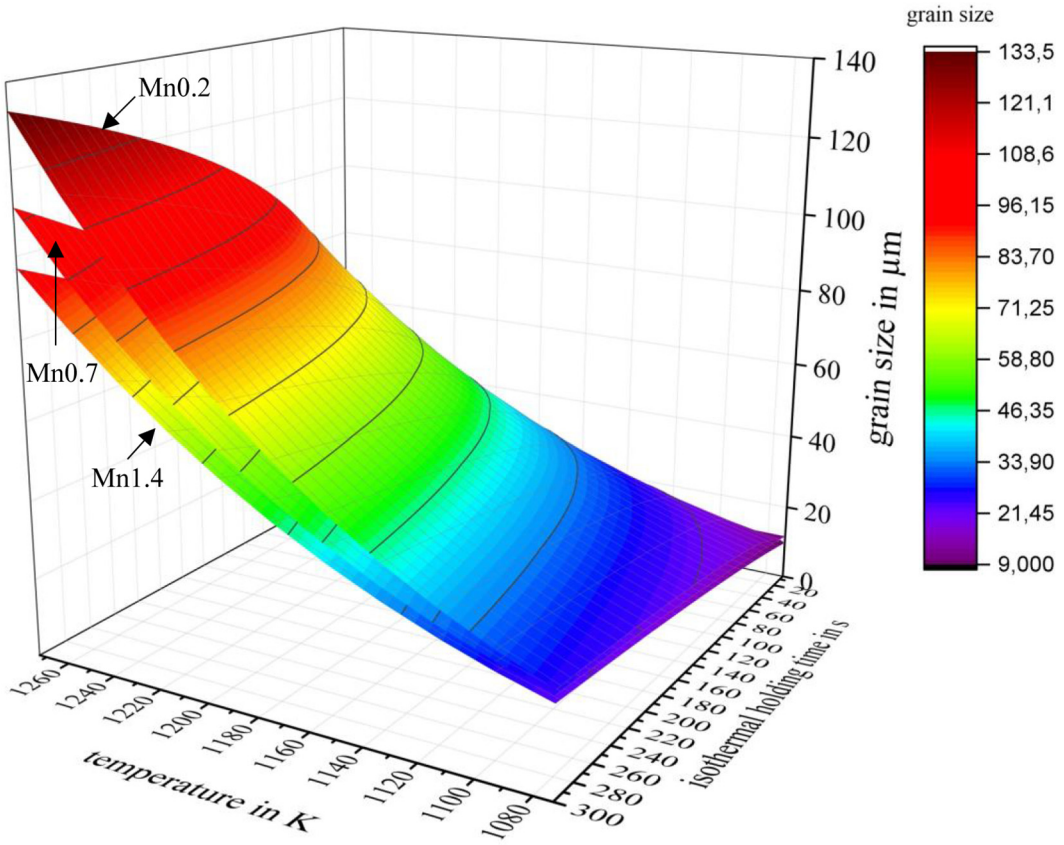

Fig. 7. Grain size development after isothermal heat treatment of steels Mn0.2, Mn0.7 and Mn1.4.

RD making this direction the favorable one regarding the soft magnetic properties. For angles of around 67° with regard to the RD, magnetic properties are worst concluding that there is no significant effect of Mn on the isotropy properties of the investigated materials. The *A* parameters, which are the integral of all A_θ values for each material shown in Fig. 12 are given in Table 2. It can be concluded that Mn can slightly improve the texture of high Si alloyed electrical steel sheets here. Increasing Mn content leads to a decreasing *A* parameter. As magnetic properties are measured in single sheet tester in 0° and 90° direction solely, the correlation of the measured magnetic properties with texture needs to be linked to $A_{0°}$ and $A_{90°}$ values which are listed in Table 2 also. In this study they have the same order like the averaged *A* parameter. Compared with results of [32], one can find some accordances: Firstly, the variation of the A_θ parameter occurs in a small range of around just 6 deg even though the theoretically range is 0–55 deg. Secondly, the *A* parameters are close to the generally observed value in industrially manufactured NO steels of 32 deg. Texture is known to affect the magnetic properties of NO electrical steels being P_h and magnetic induction the most relevant ones. Considering the regression equations from Kestens valid for 1.5 T, the hysteresis loss reduction by texture improvement evoked by Mn adaption should be around 0.077 W/kg comparing the maximum range of *A* parameters which are generated by Mn0.2 and Mn1.4. By just taking the RD and TD into account because these directions are measured in this study, the expected improvement of P_h by Mn should be 0.12 W/kg from the viewpoint of texture effect solely. The calculation for magnetic induction B_{25} leads to a calculated improvement of 8.16 mT for all directions and 13.04 mT for the measured direction in RD and TD. Of course, the B_{25} value is affected by Mn itself so the formulas here are just for the estimation of the magnitude of the consequences of different *A* parameters showing the effect of Mn on texture is small. That result fits to observations of [32]. One explanation is that the process chain for the production of the investigated material was same, including the hot rolling finishing temperature and the HSA temperature which are known as relevant factors for texture manipulation as the conventional process chain for NO electrical steel allows just very limited possibilities to control texture anyway. Further on the phase transformation was not affected by Mn which could randomize the texture. Mn has a subordinate role for texture control in high silicon alloyed steels upon condition that S level is very low at the same time. The reason might be that MnS and $MnSiN_2$ precipitation, which possibly affects the texture development, is not sufficiently affected by Mn content then. This result is in good accordance with [12] who found a similar behavior for Al variations in high silicon alloyed electrical steel sheets.

3.2. Mechanical properties

Although electrical steels are a functional material, mechanical properties need to be considered because they are crucial for the design of electrical machines. Especially, in high-speed motors with high frequencies, centrifugal forces are high. In motors with permanent excitations the ligament between the magnet and the air gap of the rotor usually receives highest stresses. Plastic deformation needs to be prevented so the yield strength needs to be high to withstand the forces in the operating machine. There are four common possibilities to increase the hardness of steels: Dislocation hardening, precipitation hardening, grain refinement and solid solution hardening. Dislocation hardening and precipitation hardening are known to deteriorate the magnetic properties of electrical steels [23,33,34]. As discussed above, grain size affects the magnetic properties and therefore it needs to be adjusted carefully which limits the scope for variations regarding mechanical properties. Finally, solid solution hardening is the mechanism of choice to improve mechanical properties without worsening the magnetic properties significantly [4,5].

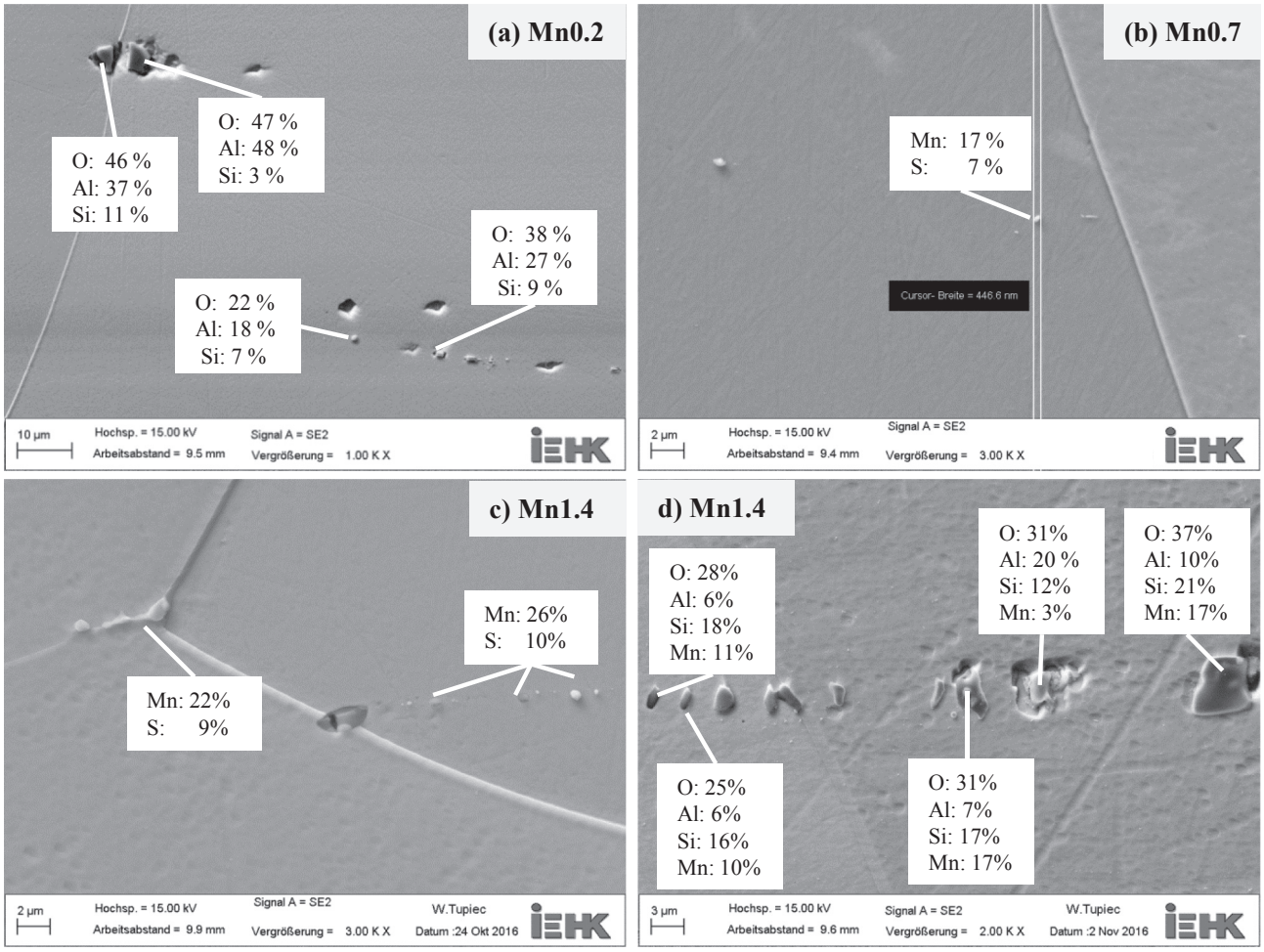

Fig. 8. SEM pictures and according chemical compositions of second phase particles measured by EDS of all steels in the fully finished state given in wt%.

Fig. 13 presents the mechanical properties of the investigated materials parallel to the RD. While yield strength and ultimate tensile strength increase with increasing Mn content, the fracture strain is almost constant. The grain size of the samples is 121 µm, 84 µm and 77 µm with increasing Mn content which needs to be considered. The average increase of yield strength is around 30 MPa per wt% of Mn. This is almost the same value that [4] observed in high Si alloyed steel and it is in accordance with the increase of tensile yield strength by Mn in pure iron [35]. The ultimate tensile strength is increased to the same extent as the tensile yield strength. It follows that Mn can be used in

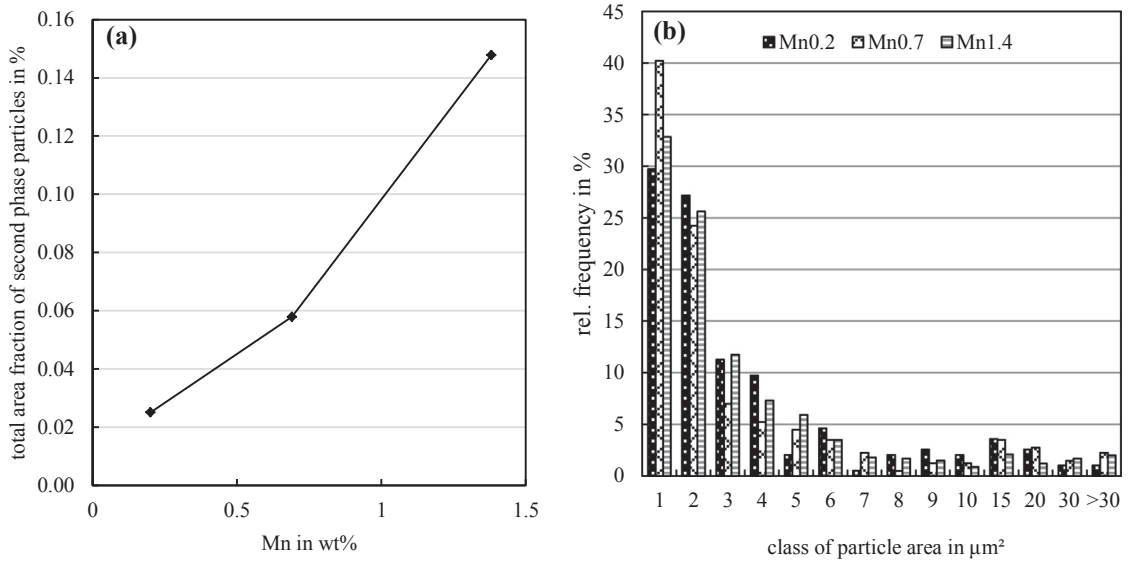

Fig. 9. Total area fraction of second phase particles in a) and relative frequency for different classes of particle size.

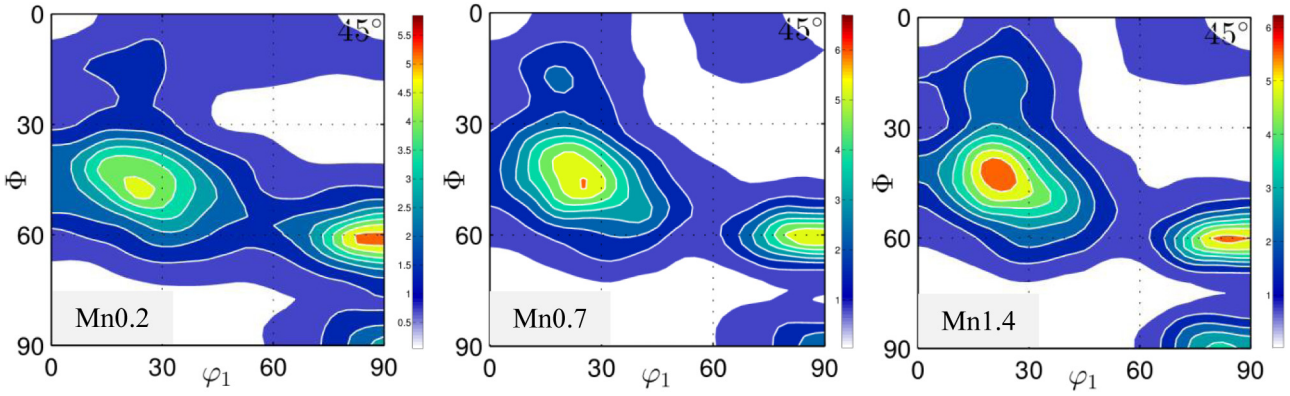

Fig. 10. $\varphi_2 = 45°$ ODF sections after final annealing (ff) at 1000 °C. Layer of measurement $S = 0.5$.

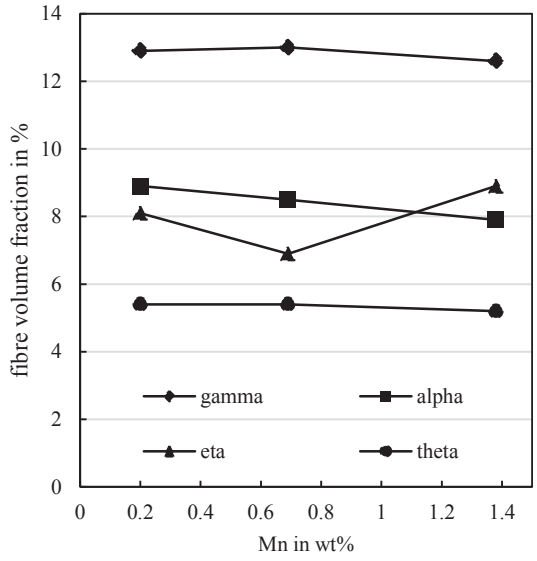

Fig. 11. Fibre volume fractions after final annealing depending on Mn content.

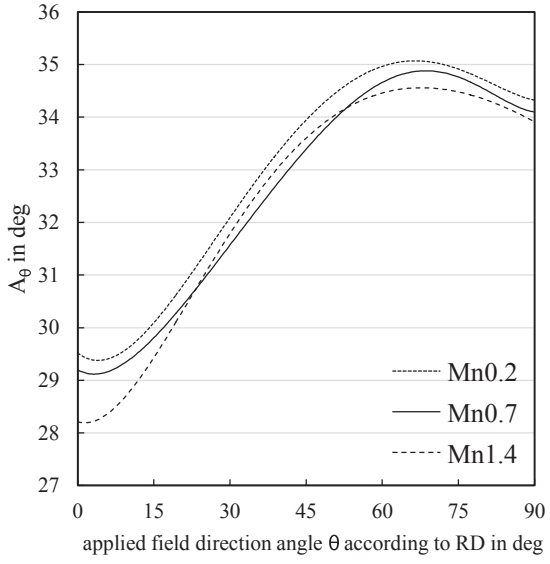

Fig. 12. Effect of Mn on A_θ texture parameter.

these steels for solid solution hardening.

3.3. Magnetic properties

The main reason for alloying of electrical steel grades is the increase of electrical resistance, because it lowers iron losses. The effect of Mn on the specific electrical resistance is given in Fig. 14. Alloying with Mn leads to a linear increase of the electrical resistance of around 0.0619 μΩm per wt% Mn in this study. This value is in good accordance with the effect of Mn in pure iron [35] but higher than the value of 0.0464 μΩm per wt% Mn calculated by [36] who measured the electrical resistance for smaller Mn contents.

Total losses P_{tot} are the sum of hysteresis losses P_h, classical eddy-current losses $P_{e,c}$ and anomalous losses P_a.

$$P_{tot} = P_h + P_{e,c} + P_a$$

The classical eddy-current losses can be calculated by Eq. (3) according to [37]

$$P_{e,c} = \frac{(\pi B_{max} df)^2}{6\rho_m \rho_e} \tag{3}$$

d is the sheet thickness, f is the frequency, ρ_e is the electrical resistance, ρ_m is the density of the material and B_{max} the maximum flux density. The increase of electrical resistance by alloying with Mn directly affects $P_{e,c}$ so that $\rho_e = f(Mn)$. As long as P_h is not determined by DC measurements, it can be approached by linear regression of $(P_{tot} - P_{e,c})/f$ (here for $f = 10$ Hz and $f = 50$ Hz) vs. $\sqrt{f}$ according to [38] as a consequence that

$$P_a = P_{tot} - P_h - P_{e,c}. \tag{4}$$

The iron losses of the investigated materials at different frequencies and inductions are shown in Fig. 15. The values are determined by single sheet tester with a fixed physical path length, which is not adapted for Epstein frame measurements with the same material, so that losses can be compared among themselves but not with Epstein frame results. Due to the measurement in RD and TD, the results are averaged and the error bar shows the min/max deviation (very small for Mn1.4). The losses are separated as described above. The shown materials have almost same grain size. This allows bringing out the direct effect of Mn on losses.

Comparing P_{tot} at different frequencies it becomes obvious that the effect of Mn is different depending on frequency. For small frequencies (10 Hz in this case) Mn causes increasing total losses as for 50 Hz P_{tot} is almost constant. For higher frequencies, Mn1.4 leads to lowest losses making Mn a suitable alloying element for high frequency applications in terms of loss reduction. The shift in the effect of Mn on losses from increasing to decreasing P_{tot} with increasing frequency can be explained by the different effects which Mn has on the three parts of losses.

Mn alloying leads to an increase of P_h. As P_h is the dominant part of

Table 2
Calculated *A* parameter from ODF texture measurements.

Material	*A* parameter	$A_{0°}$	$A_{90°}$
Mn0.2	32.97 deg	29.45 deg	34.31 deg
Mn0.7	32.62 deg	29.18 deg	34.07 deg
Mn1.4	32.46 deg	28.16 deg	33.97 deg

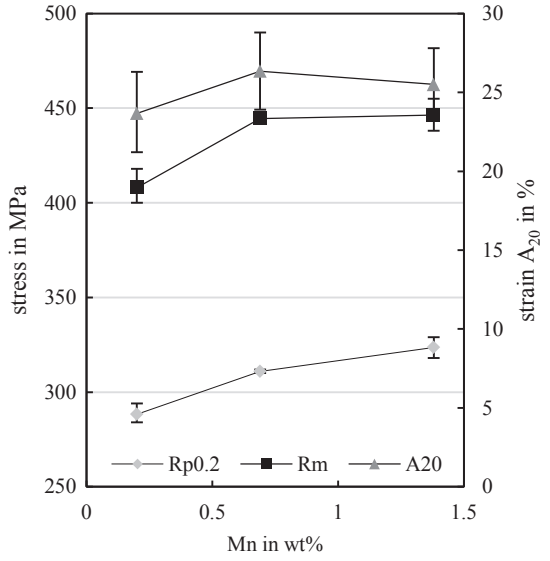

Fig. 13. Effect of Mn on mechanical properties (parallel to RD).

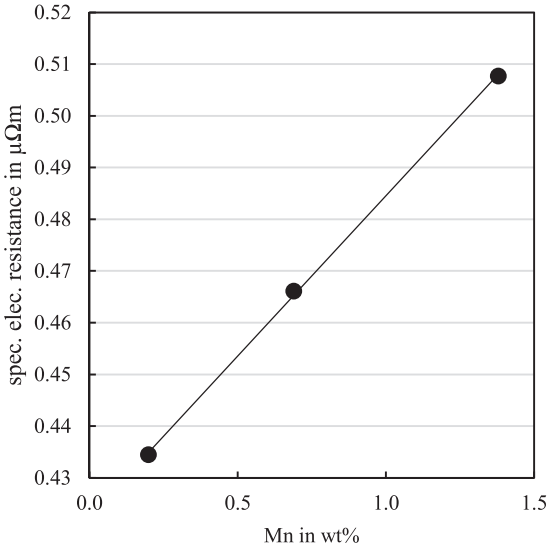

Fig. 14. Effect of Mn in high silicon alloyed electrical steel sheets on specific electrical resistance.

losses for small frequencies with around 75% at 10 Hz, Mn deteriorates the total losses in the low frequency range leading to Mn0.2 as the favorable material. The dynamic losses get more important the higher the frequency gets. For 50 Hz, dynamic losses exceed the quasistatic hysteresis losses. Even though P_{tot} is compound by different amounts of the individual loss components, P_{tot} is almost same for this frequency because Mn decreases P_a and $P_{e,c}$ which compensates the increasing P_h. For 1000 Hz measurements $P_{e,c}$ are with around 60% the dominant part of losses. Due to the increased electrical resistance by Mn addition, Mn1.4 shows lowest P_{tot}. P_{tot} can also be written as a function of f (Eq. (5)) to point out the frequency dependency. It is known that P_h has linear correlation with f, $P_{e,c}$ has f^2 correlation like shown in (3) and P_a shows a $f^{1,5}$ dependency. This makes it possible to describe P_{tot} according to [12] as

$$P_{tot} = c_h f + c_{e,c} f^2 + c_a f^{1,5} \quad (5)$$

The calculated loss parameters c_h, $c_{e,c}$ and c_a for the investigated materials depending on Mn content are given in Fig. 16. It gets obvious that Mn is suitable to decrease $c_{e,c}$ and c_a which makes Mn a sufficient element to reduce core losses.

To explain the magnetic behavior, the microstructural results and theoretical explanations need to be taken into account. Mn increases coefficient c_h. As shown in Table 2 Mn slightly improves texture. But for losses, texture is known to have a minor effect but has larger impact on permeability [32]. Other effects on magnetic losses like grain size, sheet thickness and surface quality can all be neglected because they are almost same for the compared specimens. But as shown in Fig. 9 the amount of second phase particles which can be inclusions and precipitates increases with increasing Mn content. The effect of second phase particles on P_h is known from several studies [23,39–41]. In grain-oriented materials they are suitable to delay secondary recrystallization which facilitates the formation of Goss texture. But in NO material, precipitates are usually harmful for the magnetic properties if they exceed a size of around 30 nm [23]. The observed particles might act directly as pinning sides for domain boundaries. Additionally Lee found that newly formed and hard to magnetize domains occur around particles because domain wall behavior depends strongly on local lattice distortion. This results in an increase of hysteresis losses [39]. So beside the indirect effect of Mn on magnetic properties by retarding grain growth which requires longer annealing times with increasing Mn content to adjust same grain sizes, there is also a direct way of Mn to affect c_h. The negative effect of second phase particles exceeds the slightly positive effect of texture here. It is probable that a higher oxidic purity would lead to further magnetic improvement of these steels especially to reduce P_h. In combination with very low carbon content, there are additional metallurgical measures to vacuum treatment required to decrease the oxygen content of the materials.

The effect of Mn on the complexity of the domain structure was not part of this study but nevertheless it might exist. With the help of magneto-optic Kerr microscopy it is shown in [12] that increasing alloying content causes a more complex domain structure. As alloying elements usually decrease the magnetic anisotropy K_1 [42] which is proportional to the domain wall energy, the domain wall area needs to increase to minimize the magneto-static energy. This might results in a rising number of domains by Mn alloying which causes increasing P_h. It is also known that magnetostriction is sensitive to the chemical composition of the material. For field strengths > 0.015 T, Mn increases magnetostriction for the examined range of Mn [43] which might result in a further increase of P_h with increasing Mn content. The effect of Mn on P_a is not as clear as the effect on P_h and $P_{e,c}$ because P_a increases slightly for Mn0.7 and decreases for Mn1.4 being the decrease from Mn0.7 to Mn1.4 bigger than the increase from Mn0.2 to Mn0.7. It means that alloying with Mn can be helpful to decrease P_a for sufficient Mn contents. This behavior can also results from the increase of electrical resistance which decreases anomalous losses. Further on, the mentioned domain refinement can also reduce P_a because this part of losses is known to be directly correlated to domain wall velocity which is determined by domain size.

Beside losses, magnetic induction is the other important magnetic parameter for electrical steels. It is also affected by Mn, which is shown in Fig. 17. This is due to the decrease of saturation magnetization which alloying with Mn brings on which is around

$$B_S(T) = 2.19 - 0,026 \cdot \mathrm{Mn\,wt\%} \quad (6)$$

according to [44] in pure iron. There is a slight increase of magnetic induction for Mn0.7 and a decrease for Mn1.4 but the error bar of Mn0.2 exceeds the one of Mn0.7 which suggests that the variation is

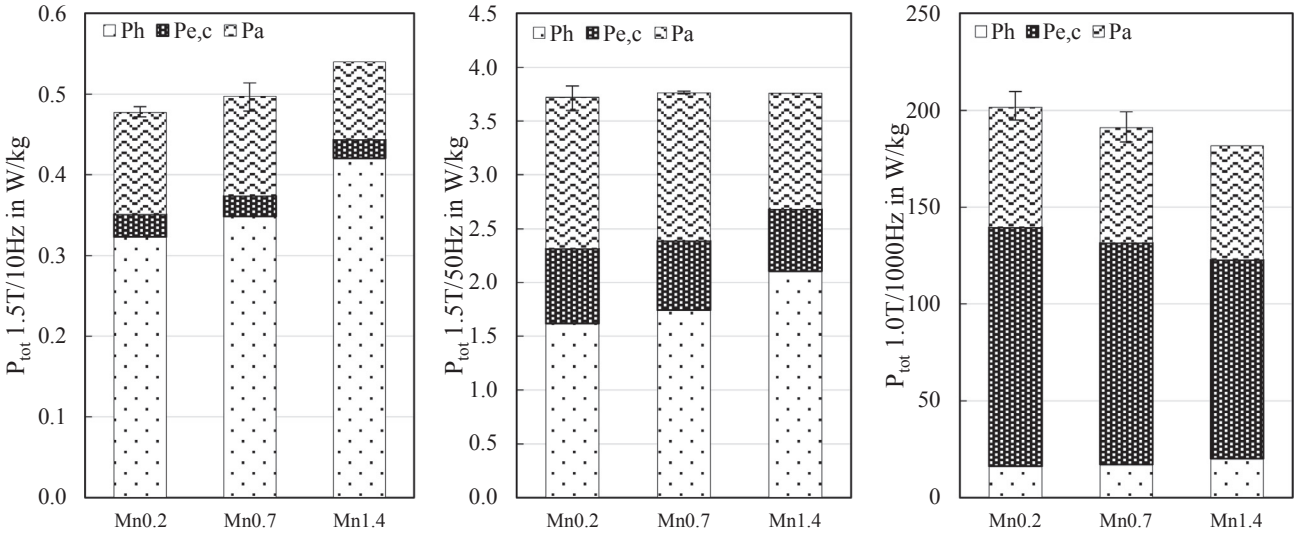

Fig. 15. Effect of Mn on total and separated iron losses at 10 Hz, 50 Hz and 1000 Hz for samples with almost same grain size of around 85 µm.

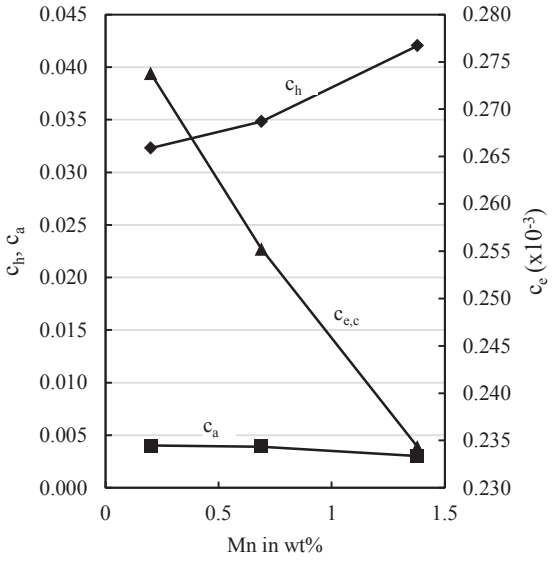

Fig. 16. Effect on Mn on loss parameters of samples with almost same grain size of 85 µm. Parameters are calculated from 1.5 T/10 Hz measurements.

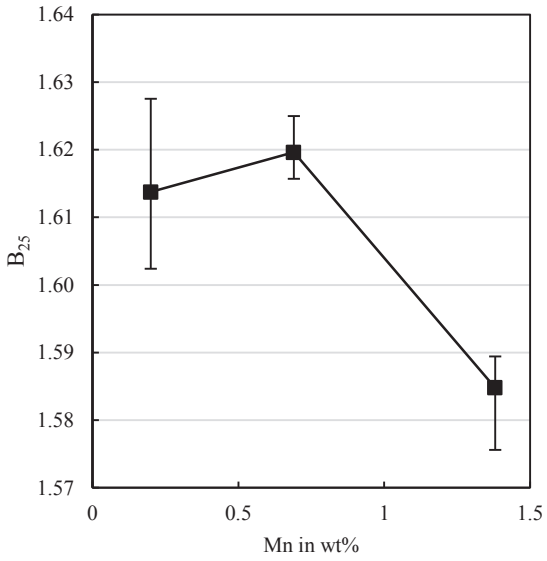

Fig. 17. Effect of Mn on magnetic induction B_{25}.

very small here. The averaged decrease of B_{25} by Mn addition is just 0,014 T per wt% Mn according to Fig. 17. With regard to the calculated effect of texture improvement by Mn on B_{25}, the deviation between Eq. (6) and Fig. 17 can be explained. It means that Mn alloying can lead to a smaller deterioration of the B_{25} values compared to the effect of Mn on B_S due to slight improvements of texture.

4. Conclusions

Based on these results about the influence of Mn in high silicon alloyed electrical steel sheets it can be concluded, that

- Up to 1.4 wt% Mn, electrical steel with 2.7 wt% Si is fully ferritic without phase transformation at technically relevant process conditions.
- Mn slows down grain growth rate which requires higher annealing temperatures or longer isothermal holding time to achieve the same target grain size.
- Final texture is slightly improved by Mn alloying which results in a lower texture *A*-parameter.
- Precipitation behavior of these steels is dominated by oxides coming from the steel making process. Small amounts of MnS can be detected even though the S level is very low.
- Mn can be used for solid solution hardening in electrical steels
- Mn rises the electrical resistance by 0.062 µΩm/1 wt% Mn which leads to lower losses for f > 100 Hz due to a decrease of the dynamic part of iron losses which makes Mn a suitable alloying element for high silicon alloyed electrical steel sheets
- Mn has little effect on magnetic induction being the effect on B_{25} even lower than on B_S

References

[1] O. Fischer, J. Schneider, Influence of deformation process on the improvement of non-oriented electrical steel, J. Magn. Magn. Mater. 254–255 (2003) 302–306.
[2] T. Moses, Opportunities for exploitation of magnetic materials in an energy conscious world, Interdiscipl. Sci. Rev. 27 (2002) 100–113.
[3] Worldsteel Association, steel statistical Yearbook (2016).
[4] T. Kubota, Recent progress on non-oriented silicon steel, Steel Res. Int. 76 (6) (2005) 464–470.
[5] F. Dorninger, High strength electrical steel from voestalpine, Proceedings of the 5th International Conference on Magnetism and Metallurgy, Ghent University, 2012, pp. 56–59.

[6] N. Zhang, P. Yang, W.-M. Mao, Through process texture evolution of new thin-gauge non-oriented electrical steels with high permeability, J. Magn. Magn. Mater. 397 (2016) 125–131.
[7] T. Tomida, T. Tanaka, Development of (100) texture in silicon steel sheets by removal of manganese and decaburization, ISIJ Int. 35 (1995) 548–556.
[8] J. Salinas-Beltran, et al., Effects of processing conditions on the final microstructure and magnetic properties in non-oriented electrical steels, J. Magn. Magn. Mater. 406 (2016) 159–165.
[9] M.F. Campos, M. Emura, F.J.G. Landgraf, Consequences of magnetic aging for iron losses in electrical steels, J. Magn. Magn. Mater. 304 (2006) 593–595.
[10] N. Leuning, et al., Effect of elastic and plastic tensile mechanical loading on the magnetic properties of NGO electrical steel, J. Magn. Magn. Mater. 417 (2016) 42–48.
[11] N. Leuning, et al., Effect of Material Processing and imposed mechanical stress on the magnetic, mechanical and microstructural properties of high-silicon electrical steel, Steel Res. Int. 87 (2016) 1–10.
[12] J. Hong, et al., Effect of Al content on magnetic properties of Fe-Al Non-oriented electrical steel, J. Magn. Magn. Mater. 439 (2017) 343–348.
[13] Pricop, V. et al.: Influence of alloy elements on magnetic properties of electrical steels. International Conference on Applied and Theoretical Electricity (ICATE), Craiova (2016).
[14] S.K. Chang, W.Y. Huang, Texture effect on magnetic properties by alloying specific elements in non-grain oriented silicon steels, ISIJ Int. 45 (6) (2005) 918–922.
[15] Oda, Y. et al. Ultra-low Sulfur Non-oriented Electrical Steel Sheets for Highly Efficient Motors: NKB-CORE. NKK Technical Review No. 87 (2002), p. 12–18.
[16] P.K. Rastogi, Effect of manganese and sulfur on the texture and magnetic properties of non-oriented steel, IEEE Trans. Magn. No.5 (1977) 1448–1450.
[17] K.C. Liao, The effect of manganese and sulfur contents on the magnetic properties of cold rolled lamination steels, Metall. Trans. A 17A (1986) 1259–1266.
[18] H. Yashiki, T. Kaneko, Effects of Mn and S on the grain growth and texture in cold rolled 0.5 % Si steel, ISIJ Int. 30 (4) (1990) 325–330.
[19] R. Cardoso, L. Brandao, M.A. Cunha, Influence of grain size and additions of Al and Mn on the magnetic properties of non-oriented electrical steels with 3 wt (%) Si, Mater. Res. 11 (1) (2008) 51–55.
[20] K. Honma, et al., Development of non-oriented and grain-oriented silicon steel (invited), IEEE Trans. Magn. No.5 (1985) 1903–1908.
[21] T. Nakayama, et al., Effects of manganese and sulfur contents and slab reheating temperatures on the magnetic properties of non-oriented semi-processed electrical steel sheet, J. Magn. Magn. Mater. 234 (2001) 55–61.
[22] P. Ghosh, et al., Effect of metallurgical factors on the bulk magnetic properties of non-orie nted electrical steels, J. Magn. Magn. Mater. 356 (2014) 42–51.
[23] K. Jenkins, M. Lindemo, Precipitates in electrical steels, J. Magn. Magn. Mater. 320 (2008) 2423–2429.
[24] T. Gladman, Grain Size Control, Institute of Materials, Minerals & Mining, London, 2004.
[25] H.V. Atkinson, Theories of normal grain growth in pure single phase systems, Acta Metal. 36 (3) (1988) 469–491.
[26] G. Gottstein, Materialwissenschaft und Werkstofftechnik, Springer Vieweg, Berlin, Heidelberg, 2014.
[27] F.X. Gil, et al., Grain growth kinetics of pure titanium, Scr. Metall. Mater. 33 (3) (1995) 1361–1366.
[28] X. Bian, et al., The effect of copper precipitates on the recrystallization textures and magnetic properties of non-oriented electrical steels, J. Alloy. Compd. 588 (2014) 108–113.
[29] C.-K. Hou, Effect of hot band annealing temperature on the magnetic properties of low-carbon electrical steels, ISIJ Int. 36 (5) (1996) 563–571.
[30] O. Engler, Introduction to Texture Analysis, CRC Press, Boca Raton, 2010.
[31] J.-T. Park, et al., Texture evolution during recrystallization in nonoriented electrical steels, Mater. Sci. Forum 550 (2007) 533–538.
[32] L. Kestens, S. Jacobs, Texture control during the manufacturing of nonoriented electrical steels, Texture, Stress Microstruct. 2008 (2008) 1–9.
[33] T. Nakayama, M. Takahashi, Effects of vanadium on magnetic properties of semi-processed non-oriented electrical steel sheets, J. Mater. Sci. 30 (1995) 5979–5984.
[34] T. Nakayama, N. Honjou, Effect of aluminium and nitrogen on the magnetic properties of non-oriented semi-processed electrical steel sheet, J. Magn. Magn. Mater. 213 (2000) 87–94.
[35] Verein Deutscher Eisenhüttenleute, Werkstoffkunde Stahl, Springer Verlag, Berlin, Heidelberg, New York, Tokyo, 1984.
[36] P. Arato, I. Boc, T. Grof, Effect of composition on the loss of non-oriented medium silicon electric steels, J. Magn. Magn. Mater. 41 (1984) 53–55.
[37] J.J. Thomson, Electrician 28 (1892).
[38] D. Kowal, et al., Comparison of iron loss models for electrical machines with different frequency domain and time domain methods for excess loss prediction, IEEE Trans. Magn. 51 (1) (2015).
[39] S. Lee, B.C. De Cooman, Effect of Phosphorus on the magnetic osses of non-oriented 2% Si steel, ISIJ Int. 52 (6) (2012) 1162–1170.
[40] Z. Lei, et al., The hysteresis properties analysis of Fe-4 wt% Si prepared by high purity metallurgy, J. Magn. Soc. Jpn. 40 (1) (2016) 8–12.
[41] H. Shimanaka, et al., Recent development of non-oriented electrical steel sheets, J. Magn. Magn. Mater. 26 (1982) 57–64.
[42] R.C. Hall, Single-crystal magnetic anisotropy and magnetostriction studies in iron-base alloys, J. Appl. Phys. 31 (6) (1960) 1037–1038.
[43] Schulze, A. Die Magnetostriktion (1928), p. 448–505.
[44] J.K. Stanley, Metallurgy and Magnetism, American Society for Metals, Cleveland, 1949.